

On the use of multiple compartment epidemiological models to describe the dynamics of influenza in Europe

Inbar Seroussi^{1,*}, Nir Levy¹, Daniela Paolotti², Nir Sochen³, and Elad Yom-Tov¹

¹Microsoft, Herzeliya 46733, Israel

²Computational Epidemiology Laboratory, Institute for Scientific Interchange, Turin, Italy

³Department of Applied Mathematics, School of Mathematical Sciences, University of Tel Aviv, Tel Aviv, Israel

Abstract

We develop a multiple compartment Susceptible-Infected-Recovered (SIR) model to analyze the spread of several infectious diseases through different geographic areas. Additionally, we propose a data-quality sensitive optimization framework for fitting this model to observed data.

We fit the model to the temporal profile of the number of people infected by one of six influenza strains in Europe over 7 influenza seasons. In addition to describing the temporal and spatial spread of influenza, the model provides an estimate of the inter-country and intra-country infection and recovery rates of each strain and in each season. We find that disease parameters remain relatively stable, with a correlation greater than 0.5 over seasons and stains. Clustering of influenza strains by the inferred disease parameters is consistent with genome sub-types. Surprisingly, our analysis suggests that inter-country human mobility plays a negligible role in the spread of influenza in Europe. Finally, we show that the model allows the estimation of disease load in countries with poor or none existent data from the disease load in adjacent countries.

Our findings reveal information on the spreading mechanism of influenza and on disease parameters. These can be used to assist in disease surveillance and in control of influenza as well as of other infectious pathogens in a heterogenic environment.

1 Introduction

Understanding the spatio-temporal spread of infectious diseases is important for designing prevention mechanisms and control intervention strategies. The modeling of the dynamics of disease spread began with compartmental models, such as the Susceptible-Infected-Recovered (SIR) model [1]. This classic model, which describes a single pathogen in a heterogeneous environment, was later extended to cases of collections of interconnected geographic areas, spatial networks and multiple strains to model common infections such as influenza, measles, and foot-and-mouth disease [2, 3, 4, 5].

Empirical data, including both epidemiological and proxy data such as postings on social media, can be fit to these models to gain better understanding of an epidemic. These models are also useful in simulating disease progression using known demographic variables and disease parameters [6, 7]. For these two purposes multiple compartments models can account for heterogeneity in the population and disease [8, 9].

*inbarser@gmail.com

Here we aim to model the seasonal spread of influenza in Europe. Seasonal spread of influenza is highly complex due to the yearly invasion, extinction and subsequent re-invasion of viral strains as well as the spatial spreading mechanism among different populations. Previous work [6, 2] studied the global spatial and temporal spread of influenza of a single pathogen as well as that of influenza-like illness (ILI), as caused by human mobility patterns. These investigations showed the importance of air transportation and local traffic in the spreading mechanism. Similarly, [10] used modeling in conjunction with transportation data to generate surveillance systems and forecast ILI rates.

However, a unified characterization of the underlying mechanisms of spread of multiple strains among multiple populations is missing. One of the reasons for this is the dearth of high resolution (spatial, temporal and biological) epidemiological data which has only recently become available.

Here we develop a multi-compartment model to estimate the temporal and spatial spread of disease and apply it to modeling of influenza in Europe. The proposed model also provides and estimate of the infection and recovery rates. Fitting observed disease load data to such a model is a challenge, due to the complexity of the model and the availability of imperfect data. Thus, we develop a new optimization technique which allow us to take into account all available data while giving lower weight to noisy data during the optimization process. This framework allows us to add constraints on factors such as the distribution of infection and recovery rates. The model we consider applies to general networks and does not require simplifying assumption on the connectivity between countries, in contrast to models such as gravity models[11]. After fitting the model to observed infection rates, we evaluate the estimated model parameters against known demographic data and virological information, gaining insights on the form of infection and recovery rates in different types of influenza.

2 The multi-compartment SIR model

The model we develop is based on the classic SIR model, due to Kermack and McKendrick[1]. The model quantifies the number of people in each of three groups in a population: susceptible (S), infected (I), and recovered (or immune) (R). The evolution within these groups is described by a system of ordinary differential equations:

$$\frac{dS}{dt} = -\beta SI, \quad \frac{dI}{dt} = \beta SI - \gamma I, \quad \frac{dR}{dt} = \gamma I \quad (1)$$

where $\beta > 0$ is the infection rate and $\gamma > 0$ is the recovery rate.

Multiple viruses and groups of sub-populations can be accounted for [3, 12] by transforming Eq. (4) to a multidimensional representation in which S , I , R , β , and γ are tensors (Eq. (2)). These tensors act as a time-dependent state representation of the entire system, reflecting its complex multidimensional evolution, where an infectious sub-population interacts with other sub-populations under the influence of multiple viruses. Each two-dimensional projection of the tensors represents different sub-groups e.g. viruses, spatial regions. We refer to this model as a multi-compartment SIR (mcSIR).

Thus, the multi-compartment model is represented by a multi-dimensional set of equations. The dynamics of the mcSIR model is represented by the following system of ordinary differential equations:

$$\begin{aligned} \frac{d\mathbf{S}}{dt} &= -\mathbf{I}\beta^\top \mathbf{S} \\ \frac{d\mathbf{I}}{dt} &= \mathbf{S}\beta^\top \mathbf{I} - \gamma^\top \mathbf{I} \\ \frac{d\mathbf{R}}{dt} &= \gamma^\top \mathbf{I} \end{aligned} \quad (2)$$

where boldface represents a tensor. This representation of sub-populations and viruses can also be generalized to other epidemic models, such as Susceptible-Infected-Recovered-Susceptible (SIRS) and Susceptible-Infected-Susceptible (SIS) models [13].

In the analysis below we consider a system of N sub-populations and V virus strains. For simplicity, we consider a diagonal model in the dimension of the strains, i.e., allowing no mutations or cross infections between virus strains. The off-diagonal elements are only with respect to infection rates between different population groups (e.g., countries).

We note that in some cases multiple solutions of the mcSIR model can be fit to the same data. Specifically, an mcSIR model with zero off-diagonal β and γ , which are identical to the single-compartment SIR model can describe the same infected time series when the recovery rates of the two models are equal and when the sum of each row β is equal to the equivalent β in the diagonal model. Under these conditions (and assuming the same initial conditions) the two solutions are indistinguishable. In such a case, given only the time series of the infected population, the non-diagonal mcSIR solution represents high mixing which cannot be distinguished from the diagonal mcSIR solution, where no mixing occurs.

3 The Lagrangian Optimization Framework

We propose a variational technique to match the observed number of infected people to the mcSIR model. The core of this technique is a scalar energy function, i.e., the Lagrangian, $L(\dot{S}, S, \dot{I}, I, \dot{R}, R)$. The stationary solution of the Lagrangian is defined by the Euler-Lagrange equations[14]. The resulting Euler-Lagrange equations are a variation of our compartment model: The SIR model (Eq. (4)) in the case of one compartment, and the mcSIR model (Eq. (2)) in the case of multiple compartments.

We add to this functional a constraint on the distance between the number of infected people as predicted by the model and the observed data. The Lagrange multiplier coefficients are learned during the optimization process. For example, in the single compartment model, the final estimated Lagrange multiplier is a weight showing to what extent the model fit provides a good representation of the data.

To simplify the problem, we reduce the variational problem to one which accounts for only the susceptible and infected people. The number of recovered people can be computed from the number of infected people over time. In principle, the number of recovered people can also be incorporated in the Lagrangian. However, since the observed data usually only measures the number of infected people, using the reduced Lagrangian for S , and I is sufficient.

The reduced Lagrangian, $L_{\text{SIR}}(\dot{S}, S, \dot{I}, I)$ of the SIR model in this case is then:

$$L_{\text{SIR}} = L_{\text{SIR}0} + \int_0^t \left[\frac{\dot{S}I - S\dot{I}}{2} + (\beta IS + u(t)) \left(I + S - S_0 - I_0 - \frac{\gamma}{\beta} \log\left(\frac{S}{S_0}\right) \right) \right] + \frac{\lambda}{2} \int_0^t (I_{\text{data}} - I)^2 dt + \lambda_2 \log P(\beta, \gamma), \quad (3)$$

where $L_{\text{SIR}0}$ is an initial condition, λ is the Lagrange multiplier constraining the similarity to the data. The model parameters are the infection rate $\beta > 0$ and the recovery rate $\gamma > 0$. The coefficient λ_2 is an optional additional constraint on the distribution $P(\beta, \gamma)$ of the infection rate β and recovery rate γ . This constraint is added if one is given information on disease parameters, for example, the range of values and their average. The Euler-Lagrange equations based on the functional in Eq. (3), for the traditional SIR model, Eq. (4) are as

follows:

$$\begin{aligned}\dot{S} &= -(\beta IS + u(t)) - \lambda(I_{\text{data}} - I) \\ \dot{I} &= \beta IS - \gamma I + u(t) \left(1 - \frac{\gamma}{S\beta}\right),\end{aligned}\tag{4}$$

where we omit for simplicity the constraint on the distribution of the parameters. The function $u(t)$ is a constraint ensuring that the invariant of the model is satisfied,

$$I + S - S_0 - I_0 - \frac{\gamma}{\beta} \log\left(\frac{S}{S_0}\right) = 0.\tag{5}$$

The Lagrangian functional for the mcSIR model is more elaborate and can be derived in a similar manner. Similar to the Lagrangian of the SIR model (Eq. (3)), we derive the reduced Lagrangian of the mcSIR model, $L_{\text{mcSIR}}(\dot{\mathbf{S}}, \mathbf{S}, \dot{\mathbf{I}}, \mathbf{I})$. The functional is as follows:

$$\begin{aligned}L_{\text{mcSIR}} &= L_{\text{mcSIR}0} + \sum_i \int_0^t \frac{\dot{S}_i I_i - S_i \dot{I}_i}{2} dt \\ &+ \sum_i \int_0^t \left(\sum_j \beta_{ij} I_j S_i + u_i(t) \right) \left(I_i + S_i - S_{i0} - I_{i0} - \frac{\gamma_i I_i}{\sum_j \beta_{ij} I_j} \log\left(\frac{S_i}{S_{i0}}\right) \right) dt \\ &+ \sum_i \frac{\lambda_i}{2} \int_0^t (I_{\text{data},i} - I_i)^2 dt.\end{aligned}\tag{6}$$

Where $u_i(t)$ is Lagrange multiplier function, enforcing a constraint on the invariant of the equation:

$$I_i + S_i - S_{i0} - I_{i0} - \frac{\gamma_i I_i}{\sum_j \beta_{ij} I_j} \log\left(\frac{S_i}{S_{i0}}\right) = 0.\tag{7}$$

The weights λ_i are the Lagrange multipliers of each country i . The values are estimated during the optimization. The resulted weights are indication of the goodness of the fit to the data for each country. The Euler-Lagrange equations for the infected population in country i , I_i , are as follows:

$$\frac{d}{dt} \left(\frac{\partial L}{\partial \dot{I}_i} \right) = \frac{\partial L}{\partial I_i}\tag{8}$$

Substituting the Lagrangian in Eq. (6), one arrives to the following equations for the susceptible in country i with an additional constraint on the similarity to the data:

$$\begin{aligned}\dot{S}_i &= - \left(\sum_j \beta_{ij} I_j S_i + u_i(t) \right) \\ &- \beta_{ii} S_i \left(I_i + S_i - S_{i0} - I_{i0} - \frac{\gamma_i I_i}{\sum_j \beta_{ij} I_j} \log\left(\frac{S_i}{S_{i0}}\right) \right) \\ &= - \sum_j \beta_{ij} I_j S_i - u_i(t) - \lambda_i (I_{\text{data},i} - I_i)\end{aligned}\tag{9}$$

Given this equation, we can find an expression for the functions, $u_i(t) = -\dot{S}_i - \sum_j \beta_{ij} I_j S_i$, at the stationary point. Similar to the infected population. The Euler-Lagrange equations for the susceptible population in country i , S_i , are as follows:

$$\frac{d}{dt} \left(\frac{\partial L}{\partial \dot{S}_i} \right) = \frac{\partial L}{\partial S_i} \quad (10)$$

Substituting the Lagrangian in Eq. (6), one gets the following equation for the infected people in country i :

$$\begin{aligned} \dot{I}_i &= \sum_j \beta_{ij} I_j \left(I_i + S_i - S_{i0} - I_{i0} - \frac{\gamma_i}{\beta_{ii}} \log\left(\frac{S_i}{S_{i0}}\right) \right) + \sum_j \beta_{ij} I_j S_i \left(1 - \frac{\gamma_i}{\beta_{ii} S_i} \right) \\ &+ \frac{\gamma_i}{\beta_{ii}} \sum_{j \neq i} \beta_{ij} I_j + u_i(t) \left(1 - \frac{\gamma_i}{\beta_{ii} S_i} \right) \\ &= \sum_j \beta_{ij} I_j S_i - \gamma_i I_i - \left(\frac{\gamma_i}{\beta_{ii}} \sum_{j \neq i} \beta_{ij} I_j \right) + \frac{\gamma_i}{\beta_{ii}} \sum_{j \neq i} \beta_{ij} I_j + u_i(t) \left(1 - \frac{\gamma_i}{\beta_{ii} S_i} \right) \\ &= \sum_j \beta_{ij} I_j S_i - \gamma_i I_i + u_i(t) \left(1 - \frac{\gamma_i}{\beta_{ii} S_i} \right) \quad (11) \end{aligned}$$

Note that the advantage of using the Lagrangian framework in the mcSIR model is that, a-priori, we do not filter the time series of countries with noisy data. We run the optimization algorithm using all available data. The algorithm finds a solution based on the existing data, giving lower weight to noisy countries. In addition, solving the mcSIR model using the Lagrangian framework makes it possible to add a constraint on the distribution of the off-diagonal infection rates, such as L_1 norm on each row of the infection rate matrix. Such a sparsity constraint can account for spatial connectivity by limiting each country to interact with only a small number of countries.

4 Results

Though there are $24 * 7 * 6 = 1008$ possible time series, in practice only 611 out of them contained sufficient data. The threshold set for the data to be considered sufficient is that the maximum of infection rate is greater than 1% during one week of data and that the total percent of infection (per week) over the entire season was greater than 20%.

The algorithm reached an average Pearson correlation between the estimated number of infected people according to the model and the WHO data of $r = 0.59$ for SIR and $r = 0.57$ for mcSIR.

The mcSIR model fit is performed for all time series including ones below the threshold of significance. The algorithm learns smaller weights (Lagrange multipliers) for the time series that are very noisy and for ones with significant missing data. Figure 1 shows the distribution of the correlation between the WHO data and the model predictions for 6 strains and 7 seasons, for the SIR and the mcSIR models in each country.

To test the assumption that the mcSIR Lagrangian assigns a lower weight to noisier data, we calculate the correlation between the quality of the fit achieved, i.e., one over the mean square error between the data and the estimated fit, and the weights estimated from the mcSIR Lagrangian framework. The Spearman correlation between the weights and the quality of the fit for the SIR model is, on average, $\rho = 0.47$ and $\rho = 0.52$ for the mcSIR model.

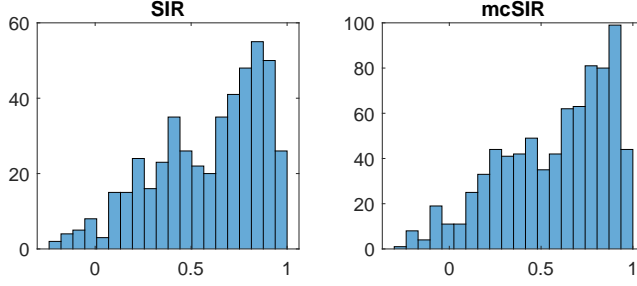


Figure 1: An histogram of the Pearson correlation between the predicted number of infected people according to the models in 369 time series over different strains and seasons and the number of infections according to WHO.

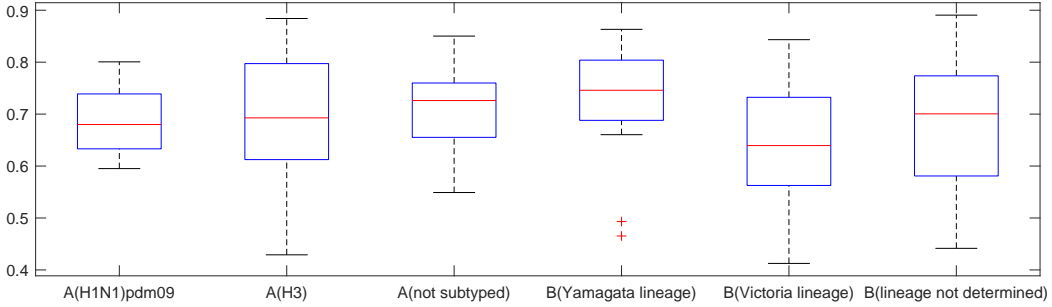


Figure 2: A box plot of the Spearman correlation between the infection rates and recovery rates for each pair of seasons of the same strain. On each box, the central mark indicates the median, and the bottom and top edges of the box indicate the 25th and 75th percentiles, respectively. The whiskers extend to the most extreme data points not considered outliers, and the outliers are plotted individually using the '+' symbol.

4.1 Infection and Recovery Rates in Different Strains and Seasons

To ascertain whether there are similarities between the inter-country estimated infection and recovery rates for each strain at each season, we calculate the correlations between parameter pairs of different seasons and strains. Each item in a pair is a vector of the inter-country parameters. Parameter pairs are considered only if they have a weight (Lagrange multiplier) greater than $1e-3$. The values of the weights are within the range 0 to 0.5. The average fraction of countries that had a weight greater than $1e-3$ is 0.84.

Figure 2 shows a box plot of the Spearman correlation between pairs of parameters extracted in different seasons for the same strain and Figure 3 shows the same among pairs of parameters extracted for different strains in the same season. As the Figures show, disease parameters among different strains and seasons are correlated. This fact is in agreement with surveillance of the spreading of influenza which indicates a similarity among seasons and strains[15, 16, 17]. We note that there is a higher correlation between diseases parameters among different seasons than among different strains. In the next section we show features of these correlations.

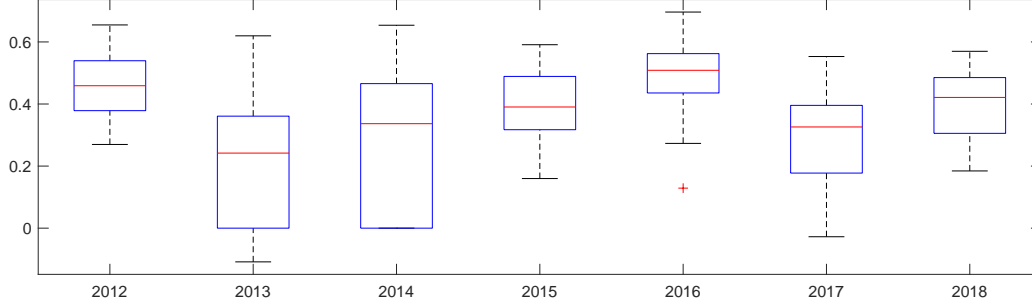


Figure 3: A box plot of the Spearman correlation between the infection rates and recovery rates for each pair of strains in the same season. On each box, the central mark indicates the median, and the bottom and top edges of the box indicate the 25th and 75th percentiles, respectively. The whiskers extend to the most extreme data points not considered outliers, and the outliers are plotted individually using the '+' symbol.

4.1.1 Parameter Similarity Among Influenza Strains

Figures 2 and 3 show that the estimated infection rates and recovery rates are correlated over seasons and strains. In this subsection, we further investigate the similarity between strains.

We use the inferred on-diagonal disease parameters to cluster influenza strains using hierarchical tree of the average Euclidean distance between clusters of data points.

Figure 4 presents dendrogram plots of this clustering over seven seasons. As the Figure demonstrates, the distances between the disease parameters estimated using the mcSIR model matches the known virological classification of the influenza virus into types. Specifically, the clustering in almost all seasons shows a separation between influenza type A and type B. We also note the similarity among A(H1N1)pdm09 and A(H3) which is present in all seasons.

4.1.2 Human Mobility and Disease Parameters

Each element of the off-diagonal infection rate matrix in the mcSIR model (Eq.(2)) describes the rate at which infected people in one country infect people in another country. A previous study [12] showed that the estimated mobile susceptible people partially explains human mobility in the US. The estimated number of mobile susceptible people are defined by the off-diagonal infection rates multiplied by the average number of infected people during an entire season. In that study, human mobility in the US explained 30% of the estimated number of mobile susceptible individuals [12].

There, to estimate the correlation between the state-level mobility patterns estimated from Twitter data and the values of β , the matrix β is normalized by the average number of infected people estimated by the mcSIR model in each country during a particular season, i.e., the infection rate matrix β is multiplied by a diagonal matrix of the average number of people transmitting the disease in a season in each country. This quantity is defined as the average mobility of the susceptible individual among different countries.

The same analysis performed on the influenza data in Europe reveals no correlation between the estimated normalized infection rates and human mobility as estimated from Twitter and as given in train and air transportation statistics. Table 1 presents the relevant Spearman correlations.

Note that the Spearman correlation between the Twitter matrix and air mobility is on average (over 6 years) 0.62. On the other hand, the Spearman correlation between the

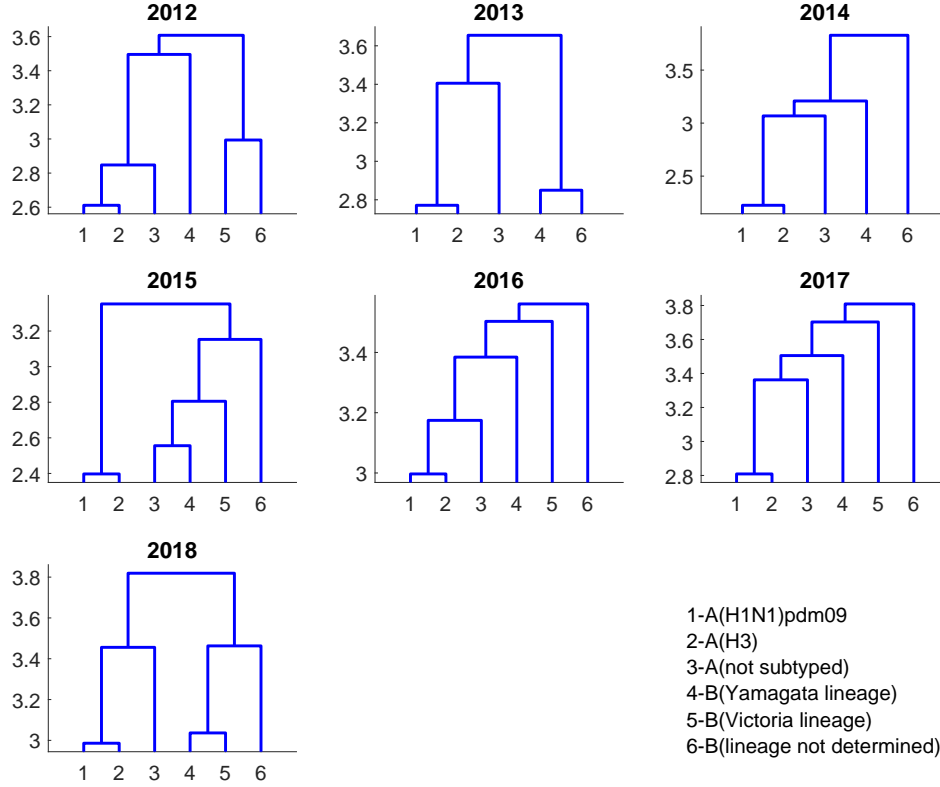


Figure 4: Hierarchical plots of clustering 6 influenza strains according to the on-diagonal coefficients in different years.

Twitter matrix and train mobility is on average (over 6 years) 0.1.

4.1.3 Data Completion using mcSIR

One of the advantages of the mcSIR model over the SIR model is the former's ability to predict the number of infected people in one country based on data from adjacent countries. In this section we demonstrate this capability by predicting the infection rate in one country based on data from the surrounding countries in the current season together with disease parameters from the country from previous season.

First, we simulate this ability (see Supporting Information C for more details). Second, we show that this idea can be implemented with real data given some prior information on the infection and recovery rates in the country containing missing data from previous seasons. Note that this is possible even though human mobility seems not to play a significant role in prediction of the infection rate in the missing country.

As an example, we simulated missing data for the United Kingdom of the influenza A (not subtyped) strain in the 2015 season. We applied the mcSIR model to data from the 24 countries, removing completely data from the United Kingdom. We initialized the number of infected people in this country to be zero. The on-diagonal infection and recovery rates were initialized to the ones approximated from the previous season.

The resulting infection rate time series estimated based on the data from other countries (without the United Kingdom) are presented in Figure 5. The Pearson correlation between the WHO data (which was not available to the model) and the mcSIR-predicted rate was 0.96 (p-value: $= 5.5 \cdot 10^{-28}$).

Table 1: Average Spearman correlation of the estimated mobility of susceptible people, as estimated by the mcSIR model fit to the data for each strain over 7 seasons. The p-value is above 0.05 in all strains, apart from three cases marked by *.

	Air mobility	Train mobility	Twitter data
A (H1N1)pdm09	0.05	-0.00	0.07
A (H3)	0.03	-0.01	0.09
A (not subtyped)	0.38*	-0.13	0.34*
B (Yamagata lineage)	0.23*	0.04	0.1
B (Victoria lineage)	0.09	0.04	0.06
B (lineage not determined)	0.00	0.00	0.1

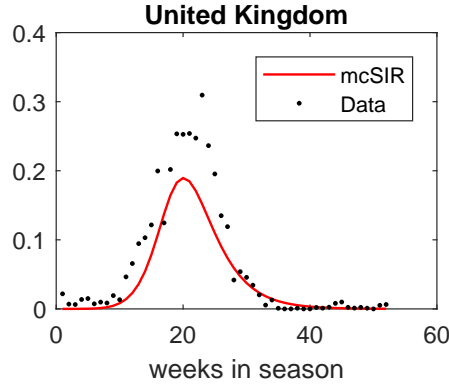


Figure 5: Estimated infection rates in the case of missing data. In red is the mcSIR-estimated infection rate in the United Kingdom, given infection rates in the other 23 countries. In dotted black is the reported infection rate in the United Kingdom.

We then repeated this simulation of missing data by rerunning the model, each time removing one country, for all strains and for all seasons from 2013 to 2017. Figure 6 shows an histogram of the correlation between the predicted infection rate (over time) in the missing country and the actual infection rate. The average correlation is 0.46 (s.d. 0.32).

The Figure shows that in most cases the model obtains a relatively high-quality prediction for the infection rate in the missing country based on neighbouring countries. Note that the distribution has a relatively heavy tail. One reason for this is that in some strains there is not enough data about other countries to provide a good predictions of the missing country. Additionally, we initiate the algorithm based on the average of the parameters over all previous seasons. Given that there is some variability between seasons (see Section 4.1), additional work is required to ascertain the number of previous seasons that should be used to estimate off-diagonal parameters.

5 Discussion

Modeling the combined spreading mechanism of multiple circulating pathogens in multiple geographic regions and among multiple populations is a challenging problem because of the dependencies between different factors affecting these regions, pathogens, and populations.

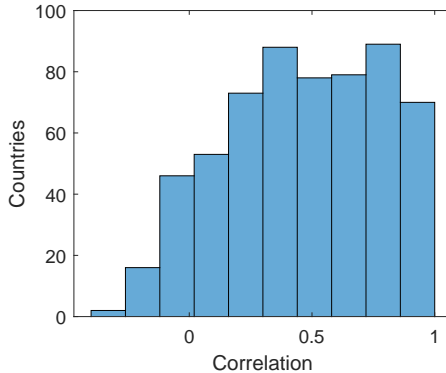


Figure 6: Histogram of the correlations between the actual infection rate in the removed country and the mcSIR-predicted infection rate. One country is removed at each time. The prediction is performed for all strains in the seasons 2013 to 2017.

In addition, the available epidemiological data is usually noisy and incomplete. Here we analyze data on seasonal influenza of multiple strains and in different countries in Europe. In order to exploit all available information and account for low-quality data we apply a new Lagrangian optimization framework. This framework enables us to estimate the infection and recovery rates using the mcSIR model while weighting differently the data from different countries. Our novel framework is general and can be applied easily to other compartment models.

Our analysis shows the importance of modeling heterogeneity in Europe, as our estimated infection and recovery rates differ for each country, as opposed, for example, to the US [12], where such differences are smaller. The parameters extracted are not independent: We show significant correlation between the inter-country infection and recovery rates in different seasons (0.6 – 0.75). In addition, we show that the distances among the disease parameters in different strains has an hierarchical structure which is consistently preserved over many season. This hierarchical structure matches genomic similarity among influenza subtypes, lending additional support to the value of these estimated parameters. In addition, as we show in the simulation, the Lagrangian framework in the mcSIR model allows us to estimate the infection rate in a country even when there is no available data on this country, simply from data of adjacent countries.

Surprisingly, the off-diagonal infected rates extracted in each season and strain are very small and uncorrelated with human mobility. This is in opposition to our finding about the significant role of human mobility in the infection mechanism of the Respiratory Syncytial Virus and West Nile Virus in the US [12]. Previous work has suggested that mobility across countries in Europe has a negligible role in disease transmission [18]. Here we find, for the first time, a direct indication that inter-country human mobility does not play significant role in the spreading of influenza over many strains and seasons of the influenza virus in Europe.

Potential limitations of this study are in the model we use, which makes significant assumptions. These include the assumption that there is no mixing interaction between strains which is known to affect the dynamics and the equilibrium state [19]. Moreover, our analysis do not addresses different social and economic groups, such as age group, which were shown to play significant role [20]. We did not account for differential vaccination rates between countries and seasons. In addition, we are limited by the resolution of the data i.e., the reported number of infected people in each country. Finer scaled data on the reported number of infected people within cites and counties may reveal more information about

the spatial spreading mechanism. Future work will focus on modeling such sub-populations within a geographic area, as well as the effects of interventions such as vaccination.

6 Materials and methods

6.1 Data Sources

6.1.1 World Health Organization (WHO) Surveillance Data

The WHO produces surveillance data for a number of emerging diseases such as Zika, Ebola, and influenza [15]. We use the weekly reported number of influenza A and B viruses classified by sub-type in Europe over the years 2012 to 2018 in the following 24 countries: France, Georgia, Germany, Spain, Italy, Austria, Denmark, Iceland, Hungary, Sweden, Turkey, Netherlands, Norway, Belgium, Portugal, Poland, Greece, Finland, Romania, Ireland, Czechia, Slovakia, Bulgaria, United Kingdom.

We define the influenza season to be one year starting at the beginning of week 41 of each year.

The sub-type taken are A (H1N1)pdm09, A (H3), A (not subtyped), B (Yamagata lineage), B (Victoria lineage), B (lineage not determined).

6.1.2 Human Mobility Data

We extracted data on air and train mobility among different countries in Europe between the years 2012 to 2017 from the Eurostat website [21].

Additionally, we collected all messages from Twitter having a GPS location in Europe from October 2015 through to March 2016. For each message, we extracted an anonymous user identifier, the time of the message, and the location from where it was made. These data comprised of approximately 50 million messages and 1.2 million users. The exact GPS location of each message was mapped as its encompassing European country. We then create a matrix of mobility, where the (i, j) -th entry of the matrix comprised of the number of people whose location in one tweet was country i and in their following tweet was country j . This matrix was normalized by dividing the number of people moving from country i to country j by the total number of people who moved from country i to any other country.

The Twitter data provide an estimate for the total movement between countries in Europe. The advantage of Twitter data over the Eurostat data is that the former provide an estimate for total human mobility, including, for example, roads, which are known to be the main source of transportation in Europe [21].

Appendix

A Fitting the Model to Observed Data

The optimization procedure is performed in two steps: First, we separately estimate the infection and recovery rates in each country, season and strain. This is done by using the Lagrangian framework of the SIR model as shown in Eq. (3). We minimize the Lagrangian using gradient descent. The estimated parameters are used as an initialization of the on-diagonal elements of the infection and the recovery rates in the mcSIR model over multiple countries for each strain and season. We then find the optimal solution of the mcSIR model using the mcSIR Lagrangian in Eq. (6). The off-diagonal terms are initialized to be the average value of the infection rates within countries divided by the total number of countries. Thus, to fit the model, $(24^2 + 24) * 6 * 7$ parameters are estimated.

The Lagrangian optimization process is performed using an alternating minimization procedure. We start with an initial guess for the fraction of infected people based on the data. We estimate the corresponding susceptible population using the Euler-Lagrange equations. The susceptible and the infected people time series found are used to minimize the Lagrangian and estimated the optimal parameters of the model. The minimum is found using the function *fminsearch* in Matlab. Using these parameters, we find a new estimate for the infected population by using again the Euler-Lagrange equations. We iterate the procedure until convergence. The advantage of using the Lagrangian framework for the mcSIR model is that it provides a way to assign smaller weights to countries with noisy data in a controlled manner while taking into account all the data available. All analyses were performed using Matlab R2017b [22].

B Fitting data using a Particle Swarm Algorithm

In order to validate numerically that our results are independent on the initial conditions, we also estimated the infection and recovery rates using an additional optimization algorithm which does not depend on the initial conditions of the single SIR model. This analysis also shows the strength of the Lagrangian framework in filtering the noisy data.

The algorithm we use is the particle swarm algorithm [23]. Particle swarm optimization is a stochastic population-based optimization method proposed by Kennedy and Eberhart [23].

We find that the results obtained using this algorithm are similar to those of the Lagrangian framework: The algorithm reached an average Pearson correlation 0.57 for SIR and 0.68 for mcSIR. There are $24 * 7 * 6 = 1008$ time series data points in practice only 287 out of them contained significant data, defined as a maximum of infection greater than 0.01 and a total infection over the season greater than 0.2.

Figures 7, 8, 9, and 10 present the results. These results are with agreement with our Lagrangian framework showing correlation between the parameters in different seasons and strains. See Sec. 4 in the main text. Note that, using the Lagrangian framework we reach better results, mainly due to the weighting mechanism provided by the Lagrange multipliers. This mechanism allows us to filter the noise in the data while learning the model parameters.

C mcSIR model completion of data based on neighboring countries

In this section, the mcSIR model is used to complete missing data in countries where the data is missing, based on information on the number of infected people in neighbouring countries. We provide two results: First, using simulated data we show that mcSIR can be used to

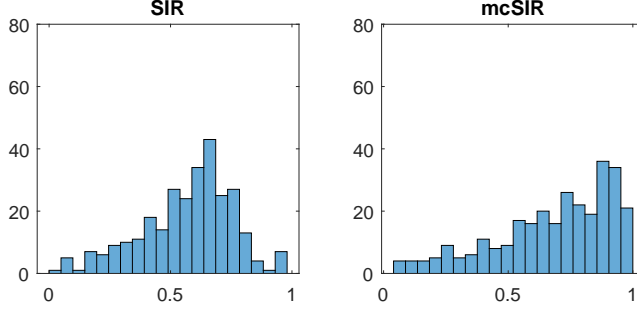


Figure 7: An histogram of the Pearson correlations achieved between the predicted infection rate in each country and WHO data, using the SIR and the mcSIR models using swarm optimization.

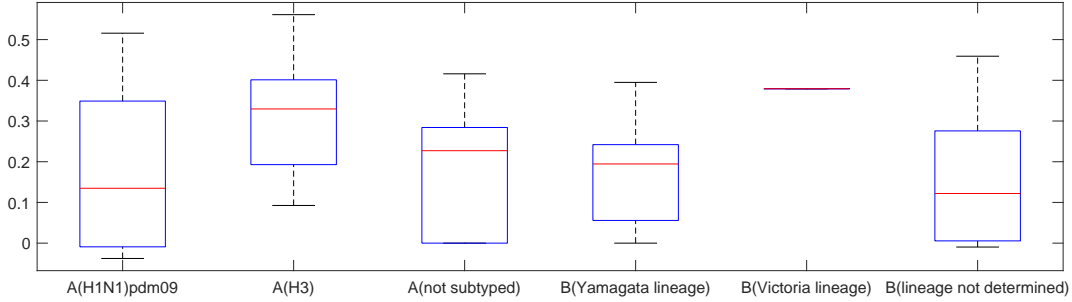


Figure 8: A box plot of the Spearman correlation between the infection rates and recovery rates for each pair of seasons of the same strain, as found using swarm optimization. On each box, the central mark indicates the median, and the bottom and top edges of the box indicate the 25th and 75th percentiles, respectively. The whiskers extend to the most extreme data points not considered outliers, and the outliers are plotted individually using the '+' symbol.

complete missing data points. Second, using real data we demonstrate the effectiveness of the mcSIR model in predicting the infection rates in countries with missing data. The results on the real data are presented in Sec. 4.1.3 in the main text.

We used the mcSIR model to simulate synthetic infection rates of 6 countries. γ_i and β_i were assigned uniformly random values for each country i in the range of $0 - 2$. The interaction between country i and j is taken to be $\beta_{ij} = \beta_i J_{\text{int}}$, and $\beta_{ii} = \beta_i(1 - J_{\text{int}})$, where J_{int} is a number between zero and one.

To simulate data quality issues, we removed random points from the data and added Gaussian noise. We also removed completely the data from one country.

The mcSIR framework with the Lagrangian solver was used to estimate the number of infected people in all countries. Figure 12 shows the results of the simulation for $J_{\text{int}} = 0.1$, here we remove 10 random points sampled without replacement and added noise with a variance of 0.04. The data from the first state was removed completely.

The average Pearson correlation between the simulated noisy data and the fitted signal was $r = 0.98$. The Pearson correlation between the simulated clean signal data in the first state and the fitted signal was $r = 0.97$. We performed the same experiment multiple times while each time removing a different set of points and increasing the signal to noise ratio.

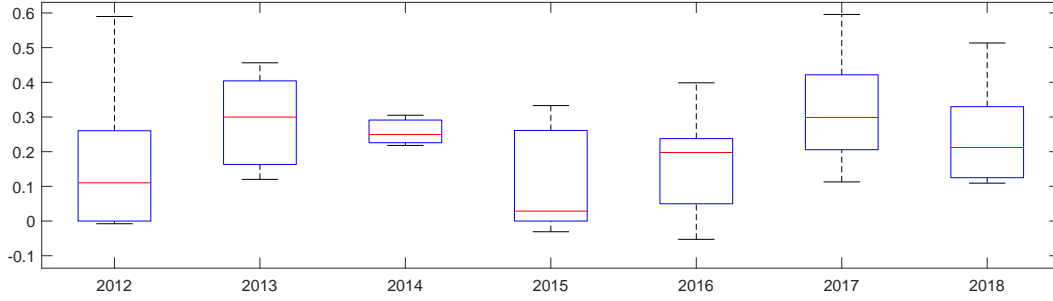


Figure 9: A box plot of the Spearman correlation between the infection rates and recovery rates for each pair of strains in the same season, as found using swarm optimization. On each box, the central mark indicates the median, and the bottom and top edges of the box indicate the 25th and 75th percentiles, respectively. The whiskers extend to the most extreme data points not considered outliers, and the outliers are plotted individually using the '+' symbol.

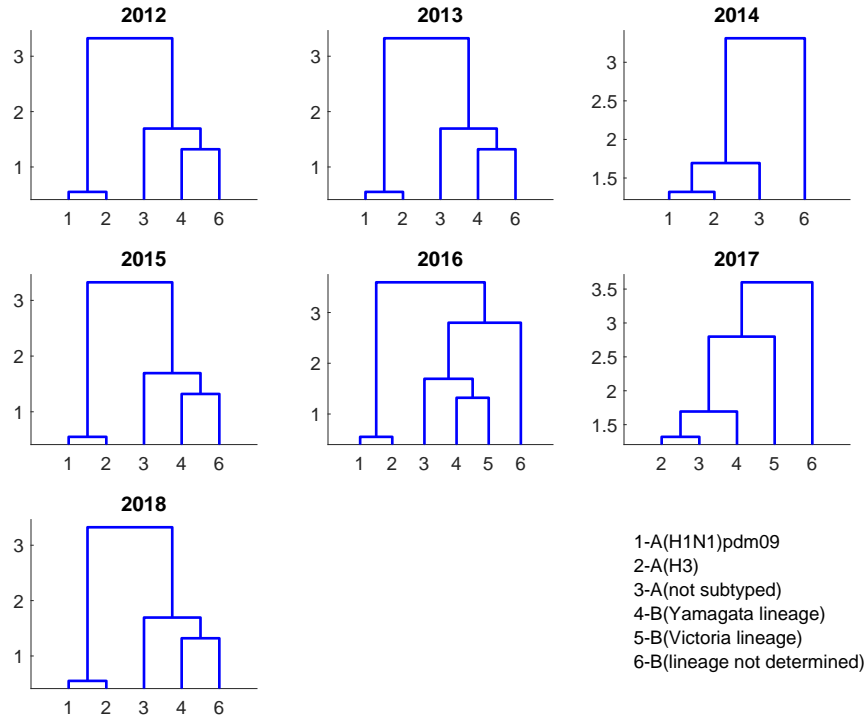


Figure 10: Linkage plots of the average Euclidean distance of the on diagonal coefficients in different years over 6 strains. The linkage tress shows separation in the estimated coefficients between strain A and strain B.

We notice that the algorithm is less sensitive to the number of points removed. On the other hand, a large perturbation in the initialization point can affect the prediction. Figure 11a shows the correlation between the predicted signal in 5 countries on which the mcSIR optimization on 6 countries was done on as a function of the variance of the added noise.

Figure 11b presents the correlation between the predicted signal in 5 countries on which the mcSIR optimization on 6 countries was done on as a function of the number of missing data point given noise variance σ_{noise}^2 . Figure 11c presents the correlation between the clean signal in the missing country and the predicted signal of this country using the mcSIR on 6 countries while performing the optimization procedure given 5 countries as a function of the variance of the added noise. Figure 11d presents the correlation as a function of the number of missing data points given noise variance σ_{noise}^2 . These results presents the robustness of the algorithm to two noise types. In addition, it shows the ability of the mcSIR model to complete for missing data based on data from neighboring countries.

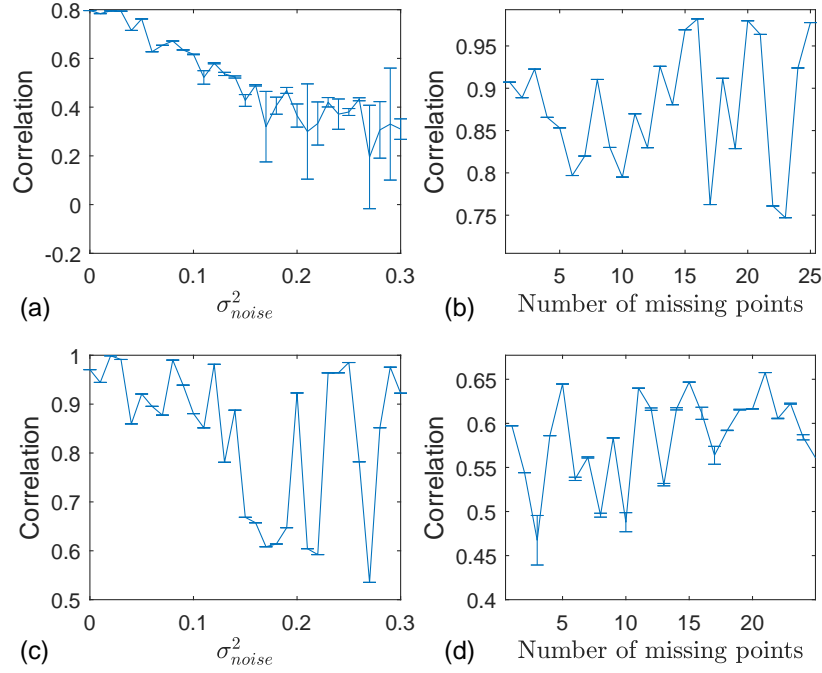


Figure 11: (a-b) The Pearson correlation between the noisy simulated data of 5 countries and the estimated infection rate time series using the mcSIR for 6 countries as a function of the variance of the added noise. In (a) the noisy data is generated by removing at random 25% of the data points at each iteration and adding noise with different variance σ_{noise}^2 . In (b) the noisy data is generated by removing a different number of random points at each iteration and adding noise with variance $\sigma_{\text{noise}}^2 = 0.1$. (c-d) The Pearson correlation between the estimated infection rate time series in the missing country using mcSIR for 6 countries and the clean data as a function of the variance of the added noise. In (c) the noisy data is generated by removing at random quarter of the point at each iteration and adding noise with variance σ_{noise}^2 . In (d) the noisy data is generated by removing at random different number of the points at each iteration and adding noise with variance $\sigma_{\text{noise}}^2 = 0.1$. The data from the 6 country is removed completely.

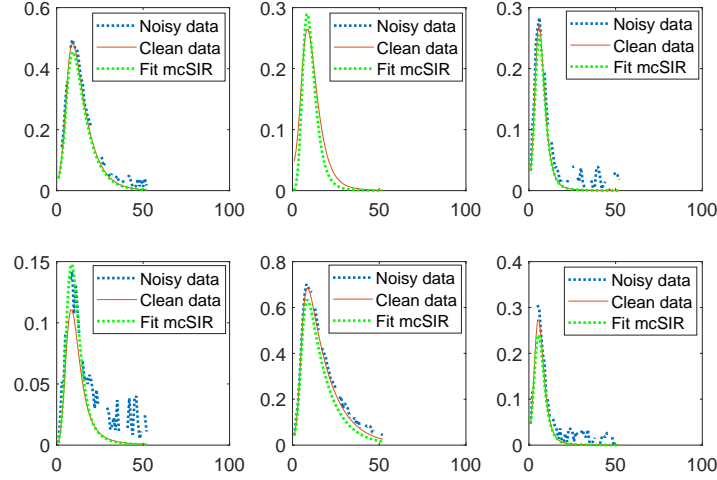


Figure 12: Results of the model fitting to mcSIR simulation over 6 countries. The data from the first state is missing. In red is the clean simulated infected rate. The green curve is the estimated solution using the mcSIR and in dotted blue is the noisy synthetic data.

References

- [1] Kermack WO, McKendrick AG. Contributions to the mathematical theory of epidemics. II. The problem of endemicity. *Proc R Soc Lond A*. 1932;138(834):55–83.
- [2] Charu V, Zeger S, Gog J, Bjørnstad ON, Kissler S, Simonsen L, et al. Human mobility and the spatial transmission of influenza in the United States. *PLoS computational biology*. 2017;13(2):e1005382.
- [3] Levy N, Iv M, Yom-Tov E. Modeling Influenza-like illnesses through composite compartmental models. *Physica A: Statistical Mechanics and its Applications*. 2018;494:288–293.
- [4] Chattopadhyay I, Kiciman E, Elliott JW, Shaman JL, Rzhetsky A. Conjunction of factors triggering waves of seasonal Influenza. *eLife*. 2018;7.
- [5] Kryazhimskiy S, Dieckmann U, Levin SA, Dushoff J. On state-space reduction in multi-strain pathogen models, with an application to antigenic drift in influenza A. *PLoS computational biology*. 2007;3(8):e159.
- [6] Colizza V, Barrat A, Barthélemy M, Vespignani A. The role of the airline transportation network in the prediction and predictability of global epidemics. *Proceedings of the National Academy of Sciences*. 2006;103(7):2015–2020.
- [7] Balcan D, Colizza V, Gonçalves B, Hu H, Ramasco JJ, Vespignani A. Multiscale mobility networks and the spatial spreading of infectious diseases. *Proceedings of the National Academy of Sciences*. 2009; p. pnas-0906910106.
- [8] Riley S. Large-scale spatial-transmission models of infectious disease. *Science*. 2007;316(5829):1298–1301.
- [9] Hagenaars T, Donnelly C, Ferguson N. Spatial heterogeneity and the persistence of infectious diseases. *Journal of theoretical biology*. 2004;229(3):349–359.

- [10] Brownstein JS, Chu S, Marathe A, Marathe MV, Nguyen AT, Paolotti D, et al. Combining participatory influenza surveillance with modeling and forecasting: three alternative approaches. *JMIR public health and surveillance*. 2017;3(4).
- [11] Sattenspiel L. *The Geographic Spread of Infectious Diseases: Models and Applications: Models and Applications*. Princeton University Press; 2009.
- [12] Seroussi I, Levy N, Yom-Tov E. Multi-Season Analysis Reveals the Spatial Structure of Disease Spread. *arXiv:190204073*. 2019;.
- [13] Keeling MJ, Rohani P. *Modeling infectious diseases in humans and animals*. Princeton University Press; 2011.
- [14] Arnol'd VI. *Mathematical methods of classical mechanics*. vol. 60. Springer Science & Business Media; 2013.
- [15] Surveillance information provided by the World Health Organization (WHO), available from;. Available from: <http://apps.who.int/flumart/Default?ReportNo=12>.
- [16] Ginsberg J, Mohebbi MH, Patel RS, Brammer L, Smolinski MS, Brilliant L. Detecting influenza epidemics using search engine query data. *Nature*. 2009;457(7232):1012.
- [17] European Centre for Disease Prevention and Control, available from;. Available from: <https://ecdc.europa.eu/en/seasonal-influenza/surveillance-and-disease-data/flu-news-europe>.
- [18] Merler S, Ajelli M. The role of population heterogeneity and human mobility in the spread of pandemic influenza. *Proceedings of the Royal Society B: Biological Sciences*. 2009;277(1681):557–565.
- [19] Garmer S, Lynn R, Rossi D, Capaldi A. Multistrain Infections in Metapopulations. *Spora: A Journal of Biomathematics*. 2015;1(1):4.
- [20] Apolloni A, Poletto C, Ramasco JJ, Jensen P, Colizza V. Metapopulation epidemic models with heterogeneous mixing and travel behaviour. *Theoretical Biology and Medical Modelling*. 2014;11(1):3.
- [21] Human mobility in Europe provided by the Eurostat Statistics Explained, available from;. Available from: https://ec.europa.eu/eurostat/statistics-explained/index.php/Passenger_transport_statistics.
- [22] MATLAB Statistics and Machine Learning Toolbox; 2017b.
- [23] Eberhart R, Kennedy J. Particle swarm optimization. In: *Proceedings of the IEEE international conference on neural networks*. vol. 4. Citeseer; 1995. p. 1942–1948.